




SCIENCE RESULTS

Planetary nebulae with UVIT: A progress report

N. KAMESWARA RAO^{1,*} , F. SUTARIA¹, J. MURTHY¹, A. RAY^{2,3} and G. PANDEY¹

¹Indian Institute of Astrophysics, Bangalore 560 034, India.

²Tata Institute of Fundamental Research, Colaba, Mumbai 400 005, India.

³Homi Bhabha Centre for Science Education (TIFR), Mumbai 400 088, India.

*Corresponding Author. E-mail: nkrao@iiap.res.in

MS received 8 November 2020; accepted 7 December 2020

Abstract. The spectral region between 1250–3000 Å contains important spectral lines to understand the morphological structures and evolution of planetary nebulae. This is the region sampled by UVIT through various filter bands both in the continuum and in emission lines (e.g.. [C IV], [He I], [Mg II] etc.). We have mapped several planetary nebulae with different characteristics, ranging in morphology from bipolar to wide and diffuse, and in various states of ionization, comparing the UV with the X-ray morphologies wherever the X-ray images were also available. The major unanticipated discovery with UVIT has been the detection of previously undetected, cold, fluorescent, H₂ gas surrounding some planetary nebulae. This may be a possible solution to the missing mass problem. Here we present a review of our studies so far done (both published and on going) with UVIT.

Keywords. Stars: AGB and post-AGB—stars: winds, outflows—planetary nebulae: ISM: planetary nebulae: general—planetary nebulae: individual: NGC 6302.

1. Introduction

Planetary nebulae (PNs) are splendid remnants of extraordinary deaths of ordinary stars in the mass range of 1–8M_⊙. They disburse the nucleosynthetically processed stellar material like carbon and s-process elements into the interstellar medium, thus enriching the matter which forms the next generation of stars. The extensive, slow, stellar wind, moving at speeds of 10 to 15 km s⁻¹, with a mass-loss rate of ~10⁻⁷M_⊙ yr⁻¹, that starts on the thermally pulsing asymptotic giant branch (AGB) – double shell (He and H) burning sources – transforms into a heavy super-wind with mass-loss rates of ~10⁻⁴M_⊙ yr⁻¹ (Delfosse *et al.* 1997) as the star evolves to the tip of AGB in the H-R diagram. In a relatively short time most of the mass is lost through a super-wind till the envelope mass falls below 10⁻³–10⁻⁴M_⊙, when a structural change occurs to the star as a degenerate CO oxygen core (which

ultimately becomes a white dwarf) develops. The photospheric radius shrinks and the effective temperature T_{eff} starts to increase keeping the luminosity almost constant. Consequently, the mass-loss rate of stellar wind decreases to about 10⁻⁸M_⊙ yr⁻¹ and the wind speed picks up to 200 to 2000 km s⁻¹. This fast stellar wind plows into the material that was earlier lost through super-wind generating a shock at the interface, while the stellar radiation heats and ionizes the ejecta. The circumstellar material starts to glow as the planetary nebula, and “illuminates the pages of the book that tells the star’s story” (Bianchi 2012). In the interacting stellar wind model (Kwok *et al.* 1978), it is the interaction of the the high speed stellar wind and the slowly expanding super-wind material that shapes the planetary nebulae. Presence of a companion and or magnetic fields may further alter the morphology of the PN. In general, PNe show very many shapes ranging from spherical to bipolar to multipolar, with some even having chaotic geometries. Morphological studies of these objects reveal their past history of mass ejections, their time scales, kinematics, properties of

This article is part of the Special Issue on “AstroSat: Five Years in Orbit”.

the ionizing source, wind interactions as well as interactions with interstellar medium etc. The UV region is important for the study of both the central stars (CSPNs) as well as the nebula, because the most important lines of the most abundant elements and their ionization states like [C II] 1335 Å, [C IV] 1550 Å, [He II] 1640 Å, [N III] 1760 Å, [C II] 2326 Å etc., fall in this region. These lines are important for modeling the ionization structure, shocked regions, chemical composition etc., and for the estimation of the T_{eff} of the hot CSPNs. Moreover, the interstellar extinction through 2179 Å bump can be studied only in the UV band. The Ultraviolet Imaging Telescope(s) (UVIT) on AstroSat (Singh *et al.* 2014), with broad and narrow band filters which cover important spectral lines and continuum with an angular resolution of about $1''.5$, over a $28'$ field-of-view, are well-suited for the study of PNs.

Details of UVIT are provided in Kumar *et al.* (2012) and its in-orbit performance is described in Tandon *et al.* (2017a) and Tandon (2020). UVIT is one of the five payloads on the multi-wavelength Indian astronomical satellite AstroSat that was launched on 2015 September 28. It consists of two 38-cm aperture telescopes, one of which is optimized for FUV, while the other has a dichroic beam splitter that reflects NUV and transmits the optical. Each UV channel can be studied in five broad and narrow band filters, as well as by low resolution transmission gratings. The Visual channel (VIS channel), which operates only in the integration mode, is used for tracking. Our project uses UVIT imaging of X-ray bright and X-ray faint planetary nebulae of different morphologies in various UV emission lines, particularly [C IV] 1550 Å, [C II] 2326 Å, [O II] 2470 Å, [Si IV] 1400 Å, [Mg II] 2800 Å, [He II] 1640 Å etc., using various filters of the UVIT–FUV and UVIT–NUV channels. We aim to study the UV morphologies, shocked regions and correspondence of UV and X-ray emissions in PNs, and to that end, several PNs of varied morphological types in both near (NUV) and far (FUV) UV ranges have been observed. Unfortunately, the NUV channel became dysfunctional after 2017. In this paper, we discuss our observations conducted so far of the selected PNs (Table 1), as well as some of the results and surprises that emerged. Detailed studies of individual objects would be presented elsewhere but some salient observational features particularly brought out by UV studies are dealt in the current presentation. Detailed discussion of NGC 40 and NGC 6302 have been presented in Kameswara *et al.* (2018a, b).

Table 1 shows a broad morphological classification of the nebulae we observed with UVIT so far which range from compact bipolar nebulae (B) to large elliptical (E) and round (R) nebulae. Some are irregular. Figure 1 illustrates typical nebular emission lines that are enclosed by UVIT filters that were used for our PN studies.

2. Results and discussion

2.1 Bipolar nebulae—FUV halos and arcs

Most of the nebulae we have observed so far belong to the group of PNe with bipolar morphology. Our sample includes NGC 40 (the “bow tie nebula”), NGC 650, NGC 2440, OH231.8+4.2 (the “Calabash nebula”), NGC 2818, Mz 3, NGC 6302 and NGC 7027. One of the reasons we observed them is to look for systematic features (aspects) in the UV that would characterise the group – e.g. the cold circumnebular H_2 gas. Detail UVIT imaging studies of NGC 40 and NGC 6302 are to be found in Kameswara *et al.* (2018a, b), while for NGC 2818 in Kameswara Rao *et al.*, A&A (submitted). Although observations of NGC 650, OH231.8+4.2, Mz3 (and IC 4997) have been done the data is not yet available from ISSDC.

The compact low excitation planetary nebula, NGC 40, was the first object we studied with a view to look for correspondence of high excitation UV line regions with Chandra X-ray images. It has been imaged in the far-ultraviolet filters F169M (UVIT/FUV-F3 with $\lambda_{\text{eff}} = 1608$ Å) and F172M (UVIT/FUV-F5 with λ_{eff} of 1717 Å), as well as in the near-ultraviolet (UVIT/NUV) filters N245M (UVIT/NUV-B13) and N279N (UVIT/NUV-N2 with λ_{eff} of 2792 Å). The filters selected would allow imaging in [C IV] 1550 Å (F169M) and [C II] 2326 Å (N245M) emission lines, as well as in the continuum (F172M) and (N263). Morphological studies in optical and infrared (IR) show that NGC 40 has ionized high density central core surrounded by faint filamentary halo with circumnebular rings that are seen only in $\text{H}\alpha$ but not in [O III]. UVIT studies show that [C II] 2326 Å emission is confined mostly to the core and shows similar morphology as low excitation lines in optical. However, strong [C IV] 1550 Å emission is present in the core and shows similar morphology and extent as that of X-ray (0.3–8 keV) emission observed by *Chandra*, suggesting interaction of the high-speed wind from WC8 central star (CS) with the nebula. An unexpected

Table 1. Target characteristics, and observation log of the PNs selected for our program.

Nebula	$\alpha, \delta(2000)$			Type ^a	Size (arcmin)	Proposal ID	Date	FUV filter	NUV filter	Comments ¹
	h m s	° ' "	''							
NGC 40	00 13 01.0	+72 31 19.1		B	0.61×0.61	G06_065	2016.12.09	F3, F5	B4, N2, Gr	A&A
NGC 650	01 42 19.7	+51 34 31.5		Br	3.2×1.97	A07_059To1	2019.10.04	F2, F3, F5		n.d.
NGC 1514	04 09 17.0	+30 46 33.5		R	1.67×1.67	G06_066	2016.12.26	F2, F3, F5	B4, B13, N2	
A 21	07 29 02.7	+13 14 48.4		E _s	10.25×10.25	G05_178T01	2016.09.30	F3, F5	B4, B13	
NGC 2440	07 41 54.9	-18 12 29.7		B, M	0.55×0.55	A07_134T02	2019.11.04	F2, F3, F5	B4, B13	
OH231.8+4.2	07 42 16.9	-14 42 50.2		B	0.5×0.83	G07_034	2017.04.04	F3, F5		n.d., ppn Calabash
JrEr1	07 57 51.6	-53 25 16.9		E _s	6.3×6.3^2	A05_103	2019.03.03	F3, F5		PNG164.8+31.1
A 30	08 46 53.5	+17 52 46.8		R _s	0.29×0.13	G06_061	2018.01.22	F2, F3, F5		Hyd.def
NGC 2818	09 16 01.5	-36 37 37.4		B	0.67×0.67	G06_068	2016.12.26	F2, F3, F5	B15, N2, Gr	A&A(p)
EGB6	09 52 59.0	+13 44 34.9		R	0.16×0.16	A05_149	2018.12.21	F2, F3, F5, Gr		(d.n.r)
NGC 3587	11 14 52.8	+55 02 00.0		R _{sm}	3.5×3.5	A09_047	2020.06.09	F1, F2, F3, F5		
Lo Tr5	12 55 33.8	+25 53 30.6		E	0.18×0.18	G08_029	2018.04.04	F1, F2, F3, F5	B4, B13, N2, B15	
MyCn18	13 39 35.1	-67 22 51.7			0.21×0.21	A05_149T03	2018.12.22	F2, F3, F5		
Mz 3	16 17 15.0	-51 59 42.2		B		G05_182	2016.06.04	F3,F5	B13, B4	$0'.5 \times 0'.5$, n.d.
NGC 6302	17 13 44.4	-37 06 11.0		B	1.0×4.85	G09_061T02	2020.06.06	F2, F3, F5		n.d., hour glass
A 70	20 31 33.2	-07 05 18.0		E	0.8×0.65	A05_103	2019.07.26	F2, F3, F5		n.d.
NGC 7027	21 07 01.8	+42 14 10.0		B	0.5×0.4	G06_071	2017.03.18	F2, F3, F5	B15, Gr, N2	A&A
Hu 1-2	21 33 08.3	+39 38 09.5		E _a	0.67×0.3	A05_103T06	2019.07.24	F2, F3, F5		n.d.
NGC 7293	22 29 38.5	-20 50 13.6		E	13.4×13.4	A07_134T03	2020.05.14	F2, F3, F5		n.d.
						A05_149T01	2018.10.05	F2, F3, F5		
						A07_059T05	2019.10.24	F2, F3, F5		
						G05_187	2016.09.30	F3, F5	B4, B13	n.d.
						G07_31	2017.07.24	F3, F5		Helix
						A07_134T01	2019.10.25	F3, F5		Position 2, n.d.
										Position 3, n.d.

The morphological classification is as follows: compact bipolar nebulae (B), large elliptical (E) and round (R). Subscripts 's', 'sm' and 'a' refer to inner structure, multiple shells and ansae respectively. Objects that have been proposed but not observed to date are noted in the last column as 'n.d.'.

^aThe types are taken from IAC Morphological Catalog of Northern Galactic Planetary Nebulae (Manchado *et al.* 1996b). ¹n.d. data is not available, Level 2 data not received from ISSDC. ²Galex FUV size is bigger -7'.

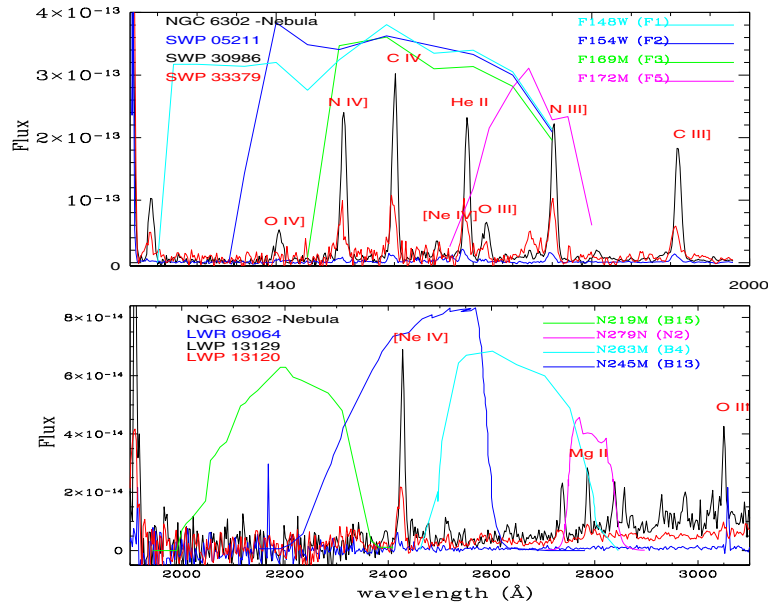


Figure 1. IUE low resolution nebular spectra of NGC6302 are shown to illustrate the wavelength range of UVIT filters. FUV is plotted on top and NUV at the bottom. Relative effective areas of various UVIT filters used for PN studies and typical nebular emission lines they include are shown.

UVIT discovery is the presence of faint large emission halo in FUV F169M surrounding the central core (Fig. 2, top). This FUV halo is absent in the other filters. This emission halo is unlikely to be due to [C IV] 1550 Å emission, or due to dust scattering. Instead, it most likely is due to UV fluorescence emission from Lyman bands of H₂ molecules since a few vib-rotational lines have already been detected in the IR from Spitzer spectra. The FUV halo in NGC 40 highlights the extensive existence of cold H₂ molecules in the regions even beyond the optical and IR halos. Thus UV studies are important to estimate the amount of H₂, which is probably the most dominant molecule and significant for mass-loss studies. Central star and the nebular core occur in the north-west edge of the FUV halo in the direction of the star's proper motion vector suggesting a possible interaction with the surrounding interstellar medium (ISM).

Presence of much bigger and more extensive FUV halo was discovered around the famous high excitation PN, NGC 6302 the butterfly nebula (Kameswara *et al.* 2018b). It has been imaged in F169M and F172M, as well as in N279N and in N219M (UVIT/NUV-B15 with λ_{eff} of 2196 Å).

Very detailed Hubble Space Telescope (HST) images have been discussed by Szyszka *et al.* (2009) who also identified the elusive central star. The optical narrow band images show two main lobes with complicated clumpy small scale structure in the East–West direction separated by a dark lane of a very dense disc

of gas (neutral and molecular) and dust, stretching to North–South. It formed into a toroid, that obscures the central star with visual extinction of about 8 magnitudes (Matsuura *et al.* 2005; Peretto *et al.* 2007; Szyszka *et al.* 2009; Wright *et al.* 2011). Meaburn *et al.* (2008) determined the distance to the nebula as 1.17 ± 0.14 kpc from expansion parallax using proper motions of features in the North–West lobe. This estimate seems to be consistent with measurements of proper motions from Hubble images of the eastern lobe (Szyszka *et al.* 2011). From 3D photoionization modelling of the nebula, Wright *et al.* (2011) derived the properties of the central star as hydrogen deficient with T_{eff} of 220000 K, $\log g$ of 7, L_* of $14300L_{\odot}$ and mass of $0.73\text{--}0.82M_{\odot}$. They also estimated the initial mass to be around $5.5M_{\odot}$.

Extensive studies of the circumstellar torus from infrared to radio wavelengths (Dinerstein & Lester 1984; Kemper *et al.* 2002; Matsuura *et al.* 2005; Peretto *et al.* 2007; Santander-García *et al.* 2017) suggest the structure is that of a broken disc containing $2.2M_{\odot}$ of dust and molecular gas expanding at 8 km s^{-1} , presumably ejected from the star some 5000 years ago, over a duration of ~ 2000 years. The torus also obscures both the star and an ionized gas disc (detected in 6-cm free–free continuum) around the star. Kinematical studies of the east and west lobes seem to suggest that an explosive event initiated a kind of Hubble flow (i.e. a flow in which the velocity increases outward in proportion to its distance from

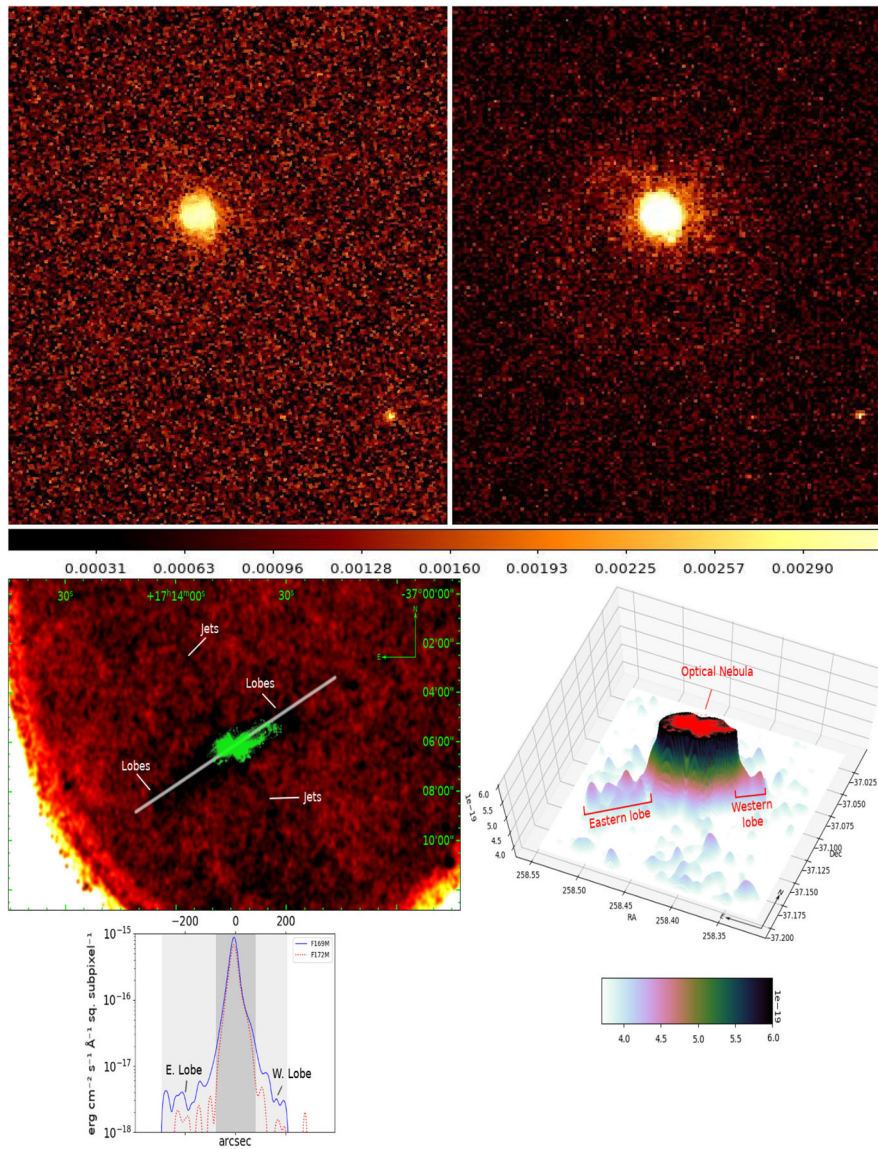


Figure 2. *Top:* FUV images of NGC 40 in F172M (*left*) and in F169M (*right*). The faint FUV halo in F169M, extending beyond the bright central region, is absent in the F172M image (Kameswara *et al.* 2018a). *Bottom:* The extensive FUV lobes and jets in NGC 6302 are shown in the F169M image which extends much beyond the optical image. The F172M image (not shown) does not show these lobes and jets.

the star) in both lobes about 2200 years back (Meaburn *et al.* 2008; Szyszka *et al.* 2009). The formation and flow of matter probably was directed by the torus into East–West lobes.

Our F169M image of this nebula shows faint emission lobes that extend to about 5' on either side of the central source. Faint orthogonal jets are also present on either side of the FUV lobes through the central source (Fig. 2, bottom). These lobes and jets are not present in either of the two NUV filters or in FUV F172M. Optical and IR images of NGC 6302 show brightly emitting bipolar lobes in the East–West direction with a

massive torus of molecular gas. Dust is seen as a dark lane in the North–South direction. FUV lobes are much more extended and oriented at a position angle of 113°. The FUV lobes and jets might be remnants of earlier (binary star) evolution, prior to the dramatic explosive event that triggered the Hubble type bipolar flows about 2200 years back. The source of the FUV lobe and jet emission is not known, but most likely is due to fluorescent emission from H₂ molecules. The cause of the difference in orientation of optical and FUV lobes is also indeterminate, although we speculate that it could be related to the binary interactions.

2.1.1 *NGC 2440*. A different kind of FUV halo is seen in the bipolar (multi-polar) PN NGC 2440 in our UVIT observations. The two prominent lobes of bipolar structure prominently seen in the optical images (e.g. HST heritage image) are resolved in the various nebular line filter images in to at least two interlocking, differently oriented, bipolar structures (Lopez *et al.* 1998). They are oriented at position angles (PA) of 35° and 85° , with a third one at 60° (Lopez *et al.* 1998). These multipolar structures suggest changes in the direction of sporadic mass outflows from the central object (Lopez *et al.* 1995; Manchado *et al.* 1996a). Many molecular emissions and outflows have been mapped. Mapping of H_2 ($v = 1 - 0S(1)$) rotational transition shows a spiky spherical structure of $\sim 73''$ diameters (Muthumariappan *et al.* 2007—personal communication; Wang *et al.* 2008) with spokes emanating from the centre. CO (3-2) emission closely follows the PA 35° bipolar axis in three clumps extending to about a radius of $\sim 36''$ from the central clump (Wang *et al.* 2008). HCN, HCO^+ emission is also detected within the nebular diameter of $\sim 71''$ (Schmidt & Ziury 2016). Cuesta and Phillips (2000a) analysed and modeled the optical nebular line filter images. Ramos-Larios and Phillips (2009) show the Spitzer images at 3.6, 4.8, and 8μ infra-red emission extending to $\sim 80''$ diameter centered on the central source where two bright nebular knots (NK and SK) separated by $\sim 6.2''$ occur and define another axis. Thus the, ionized, molecular gas and dust are all confined within $\sim 80''$ diameter centered around the centre. Lago and Costa (2016) modeled the morpho-kinematical structure with two bipolar components with PA 35° and 85° . The nebular abundances and the central star properties have been studied recently by Miller *et al.* (2019).

Our UVIT images are obtained in the FUV filters F169M and F172M as well as in the NUV filters N219M, N245M and N263M (Fig. 3). F169M includes the lines of [C IV] 1550 Å, [He II] 1640 Å close to the star whereas F172M mostly displays the continuum and a weakly, the [N III] 1760 Å emission feature. The images of N245M includes [C II] 2326 Å, N263M [Mg II] and the continuum. Comparison of UV images with optical nebular lines ground based (Lopez *et al.* 1998; Cuesta & Phillips 2000b) and HST show that N245M and N263M are very similar to [N II] 6584 Å, whereas F172M image is similar to that of continuum emission (Cuesta & Phillips 2000b) both in size as well as in the presence of the features consistent with low excitation line contribution.

However, the images obtained with F169M differ from those of the other UV filters and the optical lines. The bright central part of the image shows broadly similar to the [O III] 5007 Å image and shows the two bipolar systems at PA 35° and 85° (Fig. 4). The orientation of the central knots also is similar.

The most intriguing features of the F169M image are the faint halo extending beyond the central bright nebula in the North–East (NE), and to a lesser extent, on the South–West (SW). The faint halo extends beyond the $\sim 80''$ nebular diameter estimated from dust and molecular emission. It extends to $\sim 38''$ beyond the bright nebula on the NE side and $\sim 18''$ on the SW. The axis of this halo seem to coincide with PA 35° nebular axis. In addition, the most interesting is a thin jet that extends to $\sim 44''$ to the South–West beyond the nebula, parallel to the PA 35° axis. (The bright condensation at the southern end of the jet is a field star. It is also present in the F172M image.) The FUV halo in NGC 2440 is similar in nature to the other two systems NGC 40 and NGC 6302 and most likely caused by the fluorescent emission from cold H_2 molecules, excited by the diffuse UV radiation of the hot central star. This cold H_2 might be a product of much earlier mass loss from the system when it (or possibly, the primary) was on early AGB phase. The FUV jet might also be an earlier ejection from the binary system.

2.1.2 *NGC 2818*. The bipolar PN NGC 2818 presents a different kind of FUV emission. Instead of a FUV halo around the PN, NGC 2818 shows FUV emitting circum-nebular arcs at a distance from the nebula, possible remnants of much earlier mass ejections and mass-loss.

The PN NGC 2818 is one of the few known PNs that are members of galactic clusters which makes it possible to estimate a lower limit to the original main sequence mass from the cluster turnoff. In the case of NGC 2818 it is around 2.0 to $2.2M_\odot$. NGC 2818 is a high excitation nebula with lines of [He II], [C IV], [N V] same time strong lines of low excitation as well as vibrational-rotational lines of H_2 in the near and mid-IR. The Spitzer images in mid-IR wavelengths show dust emission extending beyond the optical nebula, particularly on the western lobe (Hora *et al.* 2006). From the optical spectral analysis the T_{eff} of the central star is estimated to be ~ 169000 K (Mata *et al.* 2016). Very detailed Hubble Space telescope (HST) images (Hubble Heritage image collection) have been discussed by Vazquez (2012) along with its

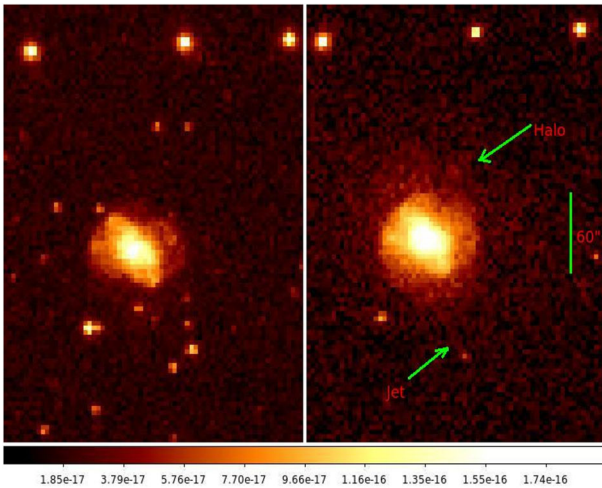


Figure 3. NUV N219M image (*left*) is compared with UVIT image in F169M (F3) of NGC 2440 (*right*).

kinematical structure. The kinematical age of the wide lobes is estimated as $\sim 8400 \pm 3400$ years. The optical narrow band images show bipolar lobes in the East–West direction with complicated small scale structure and a pinched, hourglass type narrow equatorial waist in the middle stretching to north-south. The semi-major axis is estimated to extend to $75''$ through

optical nebular lobes in East–West and a minor axis extending to $55''$ North–South with $14''$ diameter central region, which is potentially the remnant of an equatorial enhancement. A number of cometary knots are seen in images of low excitation lines e.g. [N II], that are preferentially located inside a radius of $20''$ around the central star (Vazquez 2012).

The bipolar planetary nebula, NGC 2818 and the open cluster have been imaged in three far-ultraviolet (FUV) filters, F154W: λ_{eff} of 1541, F169M: λ_{eff} of 1608 and F172M: λ_{eff} of 1717 with UVIT. The F154W image shows faint emission of a partial nebular ring and couple of nebular arcs (shell) that surround the central nebula at a distance of $370''$ and $170''$ from the central star (Fig. 5). F169M image also shows traces of these features but not as prominently as in F154W image. But the images in F172M filter, NUV from GALEX and optical filters do not show any trace of these emission features. The FUV emission from partial ring at a distance of 6.4 pc from the star suggests an ejection that took place about 60,000 years back (or more) from the central star. The observed expansion velocity of 105 km s^{-1} of the polar lobes and the distance of 3.56 kpc determined from Gaia parallaxes for both the cluster and the

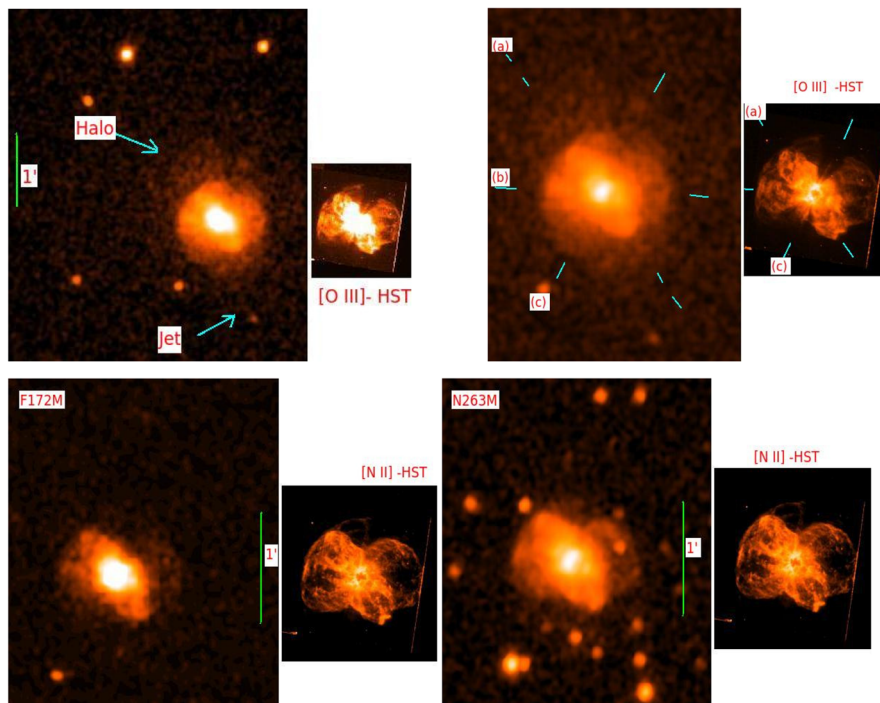


Figure 4. *Top left panel:* Images of NGC 2440 in the filter F169M (*left*) is shown along with [O III] 5007 \AA obtained with HST. The FUV halo and jet are indicated in UVIT image. *Right panel:* The same image is shown with the three bipolar orientations (PA 35° (a) and 85° (b)). *Bottom left panel:* The UVIT image of NGC 2440 in F172M is shown along with HST image in [N II] 6584 \AA . *Bottom right panel:* The UVIT image in N263M compared with the HST image in [N II] 6584 \AA is shown.

nebula suggests such an age. This is by far the most distant and oldest relic of mass ejection observed for a planetary nebula. The FUV emission in these nebular features is most likely due to UV fluorescent H_2 molecules. From the T_{eff} and luminosity of the star it appears that enough stellar UV radiation reaches the nebular arc to produce sufficient H_2 fluorescence. The original formation of the shell (or a ring) might have involved shocks or high temperature and high velocity gas, but in due course that gas has recombined and cooled to the present cold molecular gas.

The FUV images of the central bipolar nebula show bright emission region dominated by $\text{He II } \lambda 1640$ and to lesser extent $[\text{C IV}] \lambda 1550$ emission, around the star. Another prominent morphological aspect of FUV emission, particularly seen in F169M image is the presence of radial filaments (Fig. 6) diverging from the central star in almost all directions. These filaments are spread more in the direction of eastern lobe than towards western lobe. They extend to about $48''$ into eastern lobe. These filaments are much more prominent in F169M image than in $[\text{O III}]$ or F172M images, suggesting that they represent $[\text{He II}]$ (and $[\text{C IV}]$) line emitting regions. The filaments have a width of about 0.065 pc at the distance of the nebula.

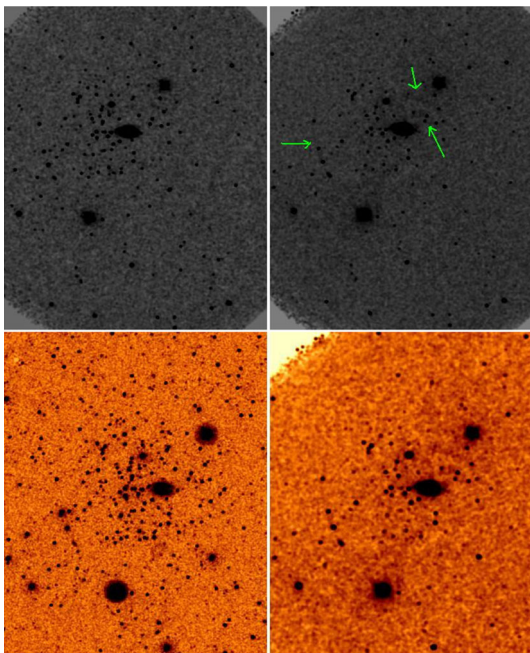


Figure 5. UVIT/FUV F154W image of NGC 2818 shows a faint, narrow, nebular, partial ring-like feature about $370''$ East of the nebula and also two nebular arcs at about $170''$ North-West of the nebula (*top right* and *bottom right*). These features are absent in F172M (*top left*) and GALEX NUV (*bottom left*) images.

This structure of the filaments is very similar to the radial rays surrounding the main ring in helix nebula as shown by O'Dell *et al.* (2004). These radial filaments seem to provide channels for the hot stellar wind to flow.

It is amazing that FUV studies could bring out relics of 60000 years past mass-loss from the pre-CSPN star of NGC 2818.

2.1.3 NGC 7027. Although our analysis of this PN is on going, we illustrate here F154W, F169M and F172M filters image (Fig. 7) from our observations and point out some interesting features. NGC 7027 (PN G084.9-03.4) – also known as the “magic carpet” nebula or “pink pillow” nebula – is located at 1 kpc (Zijlstra *et al.* 2008) and has a kinematical age of just 600 years (based on its radio flux – Masson 1989). It is a compact and young PN, one of the brightest nebulae in the sky and the most extensively studied one. NGC 7027 is a carbon-rich nebula with a very high-excitation spectrum showing lines of $[\text{O IV}]$, $[\text{Mg V}]$ etc. It hosts one of the hottest central stars known to date, with a $T_{\text{eff}} \sim 200000$ K (Latter *et al.* 2000). A small, essentially ellipsoidal, expanding ionized shell surrounds the central star (Masson 1989). Further outwards, a thin shell indicates the presence of H_2 a photo-dissociation region (PDR) and shows signs of recent interaction with collimated outflows (Cox *et al.* 2002). The nebula also shows many molecular emission lines, e.g. lines of CO , CH^+ , H_2O , and even HeH^+ ion have been detected from beyond the PDR (Wesson *et al.* 2010; Santander-García *et al.* 2017; Gusten *et al.* 2019).

The PN was discovered to be an X-ray source by Kastner *et al.* (2001), who attributed the X-ray emission to shock heating by a fast wind from the central star impacting the slow wind which the progenitor star ejected while on the asymptotic giant branch (AGB). Zhang *et al.* (2005) detected in the spectrum of this bright young PN of Raman-scattered $[\text{O VI}]$ features at 6830 \AA and 7088 \AA pointing to the existence of abundant neutral hydrogen around the ionized region

FUV is very sensitive to the internal and external extinction. NGC 7027 has high and variable extinction across the nebula that has been mapped by Walton *et al.* (1988). Montez and Kastner (2018) link the X-ray emission to the distribution of extinction across the nebula. UVIT images in FUV would reflect such extinction variations (Fig. 8) that would be explored later. UVIT images do not show presence of FUV halo or arcs as in other bipolar PNs listed earlier although

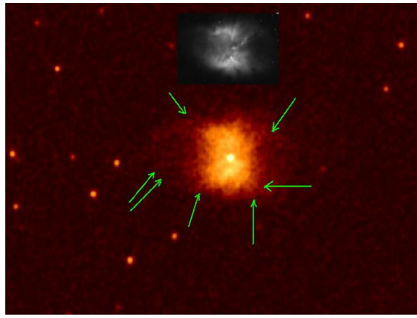


Figure 6. UVIT/FUV F169M image of NGC 2818 is compared with [O III] 5007 Å ground-based, image (*inset*: Vazquez 2012). While several features are in common, a major difference is the prominence of radial streamers (or emission filaments) in the F169M image is marked by green arrows. The bandpass of F169M filter covers mainly [He II] $\lambda 1640$ Å and [C IV] $\lambda 1550$ Å emission lines. Presence of these streamers suggest that they might have been swept up by strong stellar wind from the central star.

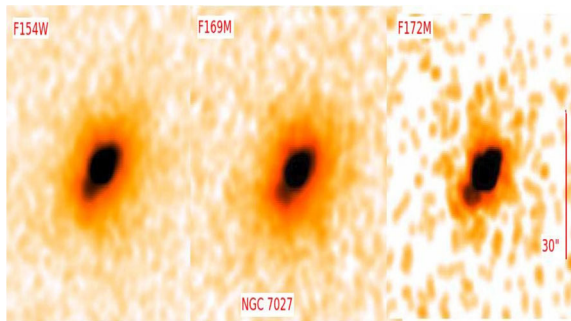


Figure 7. FUV F154W, F169M and F172M images of NGC 7027. Note that the South-East part is fainter and affected by extinction. FUV is very sensitive to dust extinction. The differential extinction can be studied from UV images.

deep images in optical (HST) do show faint circular rings around the main nebula. One possible reason is that because of high internal extinction no UV photons from the central star reach to the outer H₂ region.

2.2 Round nebulae—FUV halos

The members of this group that were observed by UVIT are NGC 1514, A 30, EGB 6, and NGC 3587

2.2.1 NGC 1514: Shining fluid! Observing NGC 1514 on 1790 November 13, William Herschel called it ‘a most singular phenomenon!’ This PN is unusual because of its very bright central star and large diameter low surface brightness nebulosity. The observation by Herschel is termed as ‘an important

event in the history of astronomy’ (Seaton 1980) because of his realisation that ‘we therefore either have a central body which is not a star or have a star which is involved in a shining fluid, of a nature totally unknown to us’ (Seaton 1980). It turns out that there is not one star at the centre but two, a sdO + A0III. Recent observations show that the binary system has a period of 3306 days and eccentricity of 0.46. The estimates of the mass for the cooler secondary is about $2.3M_{\odot}$ and the hot primary is of $0.9M_{\odot}$ (Jones *et al.* 2017).

Ressler *et al.* (2010) described the morphological structure of NGC 1514 (see their Fig. 1) as a nebula with two shells, inner and outer with diameters of 132" and 183". The inner shell has numerous bubble structures at its edge pushing into the outer shell. The monochromatic optical images of NGC 1514 show that the amorphous appearance of the nebula contains very little nebular emission within about 30" of the nucleus (Balick 1987). This is also confirmed by the absence of [C III] $\lambda 1909$ emission which is normally the strongest nebular feature in IUE spectra of PNe (Ressler *et al.* 2010).

A pair of infrared bright axisymmetric rings that surround the visible nebula were discovered by Ressler *et al.* (2010), particularly dominant in 22 μ m. Such a structure is not suggested in any of the visible wavelength images which is probably resulted from binary interaction. NGC 1514 is also a X-ray source (Tarafdar & Apparao 1988; Montez *et al.* 2015).

We have obtained UVIT images in F154W, F169M, F172M as well as in N245M, N263M, and N279N. Although our analysis is ongoing and not complete, we present few images and show the comparison with the optical image (a combination of *B*, *V*, *R* + *I* – Ressler *et al.* 2010) in Fig. 7. The UV emission seem to be mostly to the inner shell. There is UV (nebular) emission within 30". The nebular extent in FUV is less than that in near UV and optical. There seems to be streams connecting the central region to the inner shell particularly in F245M. The structure in NUV F245M is very similar to the optical except the bubbles look sharper.

2.2.2 Born-again planetary nebula A30. Abell 30 (PNG208.5+33.2, A30) is archetypal born-again PN of about 2 arc minute diameter. The central star of A30 is believed to have undergone a very late thermal pulse (VLTP) that caused the ejection of hydrogen deficient material, prominently seen in the light of [O III] lines, about 850 years back. The inner parts of the nebula are filled with this material whereas the



Figure 8. FUV F154W image (left) is shown along with the X-ray (Kastner *et al.* 2001) and HST optical image (right). The faint circular rings seen in the optical image are absent in FUV image.

outer rim of the nebula is of H-normal composition and of about 12500 years of age. A30 is also an X-ray source showing both a diffuse source covering the inner few arc seconds covering the hydrogen deficient knots and a point source located on the central star.

Born-again planetary nebulae (PNe) are believed to have experienced a VLTP (Iben *et al.* 1983) while the star was descending the white dwarf cooling track. During this event, the remaining stellar helium envelope reaches the critical mass required to ignite its fusion into carbon and oxygen (e.g., Herwig 2005; Miller Bertolami & Althaus 2006; Lawlor & MacDonald 2006); the sudden increase of pressure leads to the ejection of the newly processed material and, as the stellar envelope expands, its temperature decreases and the star returns in the Hertzsprung–Russell (HR) diagram to the locus of the asymptotic giant branch (AGB) stars. Soon after, the contraction of the envelope will increase the stellar effective temperature, boosting the UV flux, and giving rise to a new fast stellar wind. So far, the only bonafide born-again PNe are Abell 30 (A 30), Abell 58 (A 58, Nova Aql 1919), Abell 78 (A 78), and V4334 Sgr (the Sakurais object). Among them, A30 and A78 are the more evolved ones, with large limb-brightened, H-rich outer nebulae surrounding the H-poor, irregular-shaped structures that harbor the cometary knots in the innermost regions (Jacoby 1979; Hazard *et al.* 1980; Meaburn & López 1996; Meaburn *et al.* 1998). HST images in the [O III] emission line of the central regions have revealed equatorial rings (ERs) and compact polar outflows (POs) in the central regions of both PNe (Borkowski *et al.* 1993, 1995). The dynamics are revealing: while the outer nebulae show

shell-like structures expanding at velocities of 30 to 40 km^{-1} , the H-poor clumps present complex structures, with velocity spikes of 200 km^{-1} (Meaburn & López 1996; Chu *et al.* 1997; Meaburn *et al.* 1998). The morphology and kinematics of the H-poor knots unveil rich dynamical processes in the nebulae. The material photo-evaporated from the knots by the stellar radiation is swept up downstream by the fast stellar wind, which is otherwise mass loaded and slowed down (Pittard *et al.* 2005). The interactions are complex, resulting in sophisticated velocity structures, as well as X-ray emitting hot gas (Chu & Ho 1995; Guerrero *et al.* 2012; Toalá *et al.* 2015).

To study the correspondence of UV emission with the X-ray emission as well as the hydrogen deficient ejecta, we imaged A30 with UVIT in 3 FUV and 2 NUV filters. Two FUV filters, F154M (F2) and F169M (F3; λ_{eff} 1608 Å) transmit the high excitation lines of [He II], [C IV] etc. as shown in Fig. 1). The other FUV filter F172M (F5 with λ_{eff} 1717 Å) allows mostly the nebular continuum. The NUV filters N219M (B15 with λ_{eff} 2196 Å) and N279N2 (N2 with λ_{eff} 2796 Å) allow mostly low excitation lines or continuum. The images of the nebula in these filters are shown in Fig. 9. The nebula is most intense in F169M and F154W where [He II] line emission dominates. The UVIT provides a spatial resolution of $\sim 1.''3$. In the present work, we contrast the UV images with both X-ray contours as well as ground based [O III] and H-alpha images (Arturo Machado – personal communication). In the FUV F2, F3 images, the hydrogen deficient nebular knots are not as conspicuous as in the [O III] image (Fig. 8). The FUV F2, F3 show radial streamers, which are quite prominent almost extending from central region (Fig. 10) to the edge of the nebula. They provide the channels for the material photo-evaporated from the knots by the stellar radiation is swept up downstream by the fast stellar wind, which is otherwise mass loaded and slowed down (Pittard *et al.* 2005). At the edge of the channel where it interacts with the nebular boundary, arch type structures are seen suggesting that the boundary is being pushed out by the flow of stellar wind swept material. X-ray emission has been detected within A30 (e.g., Guerrero *et al.* 2012; Kastner *et al.* 2012; Montez *et al.* 2015). This born-again PN has been studied with ROSAT (PSPC and HRI), Chandra, and XMM-Newton X-ray satellites (Chu & Ho 1995; Chu *et al.* 1997; Guerrero *et al.* 2012). Its X-ray emission originates from the CSPN, but there is also diffuse emission spatially coincident with the

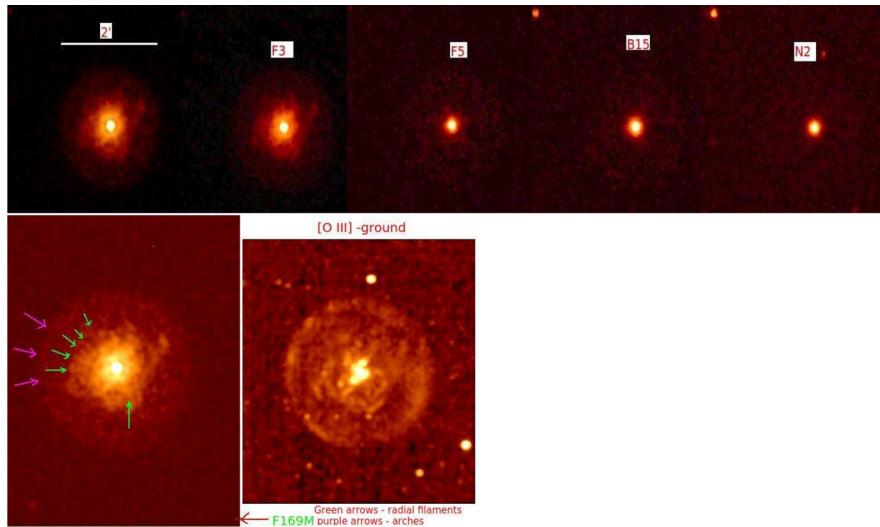


Figure 9. *Top:* PN A30 in various UVIT FUV and NUV filters is shown. *Bottom:* The UVIT/FUV F169M image of PN A30 (*left*) is compared with ground-based [O III] image (*right*). The knots and cometary tail-like filaments in the centre of the [O III] image appear to have counterparts in the F169M image. The [O III] image was supplied by Arturo Manchado (personal commun.).

clover leaf-shaped H-poor structure detected in [O III]. The X-ray emission from both the CSPN and the diffuse extended emission is extremely soft. The XMM/Newton X-ray continuum contours (Chu *et al.* 1997) are shown in Fig. 11 superposed on F169M image. They are confined mostly to the inner nebular region where the [He II] dominated gas is present. The Chandra X-ray region is displayed in Fig. 11 as an inset displaying the HST image of the inner 10'' radius of the nebula. The X-ray region contains both diffuse emission and knots.

2.2.3 FUV halo. The most surprising result of our UV imaging of A 30 is the presence of a FUV halo in the F154M and F169M filters, extending beyond the known optical and NUV nebular size (Fig. 9). The halo is not present in the F172M image, nor in any of the NUV images or even in the optical images. This situation is similar to that in NGC 40, NGC 6302 and NGC 2440. The FUV emission is very likely, the result of H₂ molecular fluorescent emission from the AGB ejecta, from molecules excited by the diffuse UV radiation from the CSPN seeping through to the cold molecular region. In spite of the presence of a very hot central star, with T_{eff} of 115000 K (Toalá *et al.* 2015), and an earlier excursion to hot PN stage (born-again), the nebula seems to still possess some unionized molecular gas. Is this gas a survivor of 12000 years of the PN evolution? The FUV halo seem to be distributed asymmetrically only on one side of the nebula. Earlier, Dinerstein and Lester (1984)

discovered an infra-red disk inside the nebula. A possible connection of this dust disk to the FUV halo needs to be explored.

2.2.4 NGC 3587—the owl nebula. This is a well studied PN with an angular size of $\sim 3'$ and of symmetrical morphology consisting of triple shell structure with a round double shell which forms the main bright nebula, and a faint outer halo (Chu *et al.* 1987; Chu *et al.* 1993; Guerrero *et al.* 2003). The bright inner shell is about $182'' \times 168''$ and resembles the face of the owl with each eye being of $\sim 35''$. The outer shell is almost circular with a diameter of $\sim 208''$. The outer shell is about 25% larger than innershell. The surface brightness of the outer shell decreases outward in H α and [O III]. It shows a limb brightening along the PA -15° to 13° and in PA 180° to 230° .

The halo is prominent in [O III] images than in H α or [N II] but is present in all the optical images (Hajian *et al.* 1997). This behavior is also common to other PN halos and is most likely an effect of the hardening of ionizing radiation (Guerrero & Manchado 1999). At the faintest level the halo is circular with a radius of $350''$ (Guerrero *et al.* 2003) although overall morphology is asymmetrical (Fig. 10). The halo is kinematically independent of the main nebula (Chu *et al.* 1998). The relative line strength in the halo are also different from the main nebula. The [N II]/H α ratio of the halo is a factor of 4 higher than the other parts of the main nebula which indicates that the halo is photo-

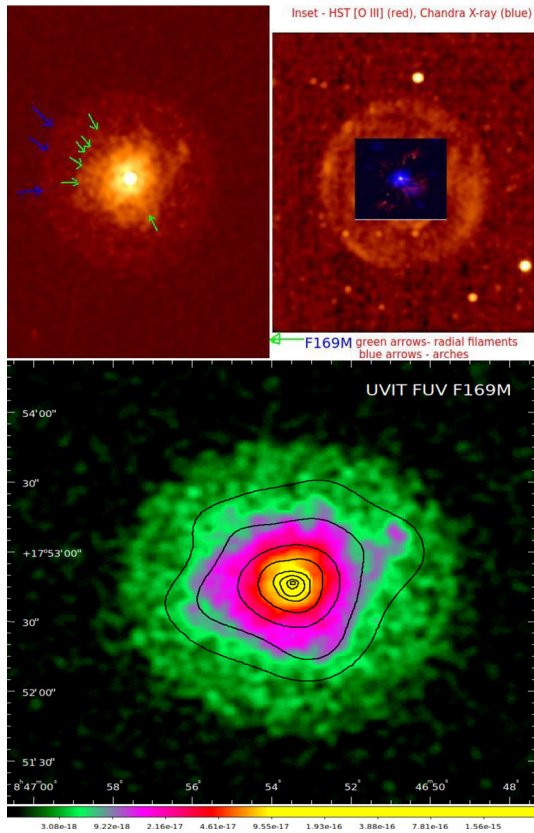


Figure 10. *Top left:* A30 image in F169M showing radial streamers from CSPN showing channels of streaming stellar wind (green arrows). The pink arrows point to the arches where the channelled flow hit the outer boundary. *Right:* Ground-based [O III] image superposed by an inset showing the region of Chandra X-ray emission (Guerrero *et al.* 2012). *Bottom:* Image of A30 F169M superposed by the XMM Newton X-ray continuum counters.

ionized. The morphology of the halo suggests an interaction with the surrounding interstellar medium and the gas in the halos is ionized by stellar UV radiation leaking through the material of the main nebula (Guerrero & Manchado 1999; Guerrero *et al.* 2003).

IUE spectra obtained 1'.5 away from the central star, almost into the halo, still show weak [He II] 1640 Å and [C III] 1909 Å. The halo gas is clearly ionized but of low density. The hot CSPN with $T_{\text{eff}} = 104000$ K and $\log g = 7.0$ shows weak stellar wind (Werner *et al.* 2019; Garcia-Diaz *et al.* 2018). A detailed spatio-kinematical study was presented by Garcia-Diaz *et al.* (2018), who treat the owl kind of nebulae as a separate class. One of the puzzles presented by the owl is the existence of cavities (the eyes of the owl) and how are they maintained. At a Gaia distance of 880 pc, the halo extends to 0.4 pc from the central star.

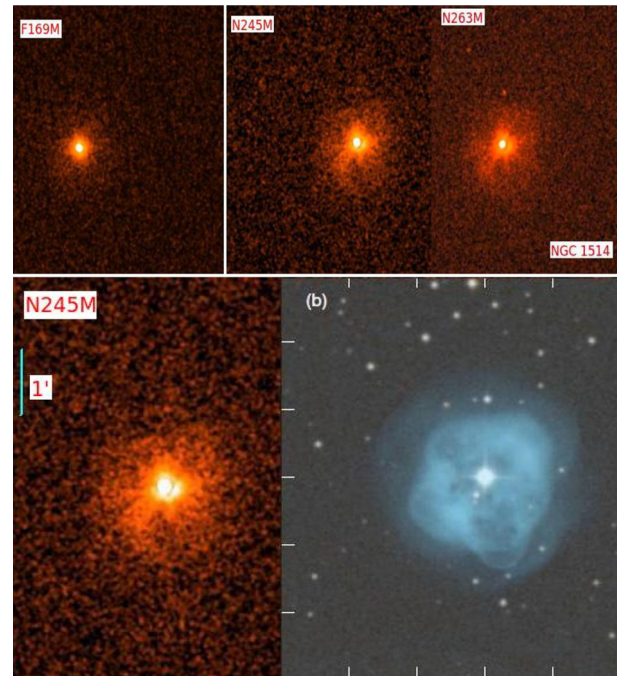


Figure 11. *Top:* FUV UVIT F169M (*left*), N245M and N263M (*right*) images of NGC 1514. The nebula is brighter in NUV N245M than in FUV F169M. *Bottom:* The UVIT N245M image of NGC 1514 is compared with optical image (*bottom right*) (Ressler *et al.* 2010). The UV emission is confined to the inner ring and centered around the central star.

Halo expansion velocity is assessed as about 10 km^{-1} (Guerrero *et al.* 2003) which suggests an age $>40,000$ years. The time scales indicate that the main nebula consists of super-wind from AGB phase and the faint halo from an early AGB wind.

Our observation with UVIT consists of FUV images in F154W, F169M, and F172M. We coupled these with the NUV image from GALEX (GI6-015012-PK148p57d1pp-nd-int), and compare them with image in the optical narrowband H- β and [N II] filters. Images in all filters show the same general features as in the optical – i.e. the two shells, and halo. However, the cavities (the eyes) are not as prominent in the FUV as in optical. Moreover, the NUV image shows a sharp wiggly boundary on the North–East showing the interaction with ISM in the direction of motion. The south western side is more diffuse and faint but more extended than NE. The FUV F169M image possibly dominated by [He II] emission, shows a more diffuse but brighter halo that extends all around the outer shell similar to NUV. The asymmetrical distribution of the halo does suggest interaction with ISM.

One of the special features seen in the F169M image is a jet in the North–West cavity (see Fig. 10)

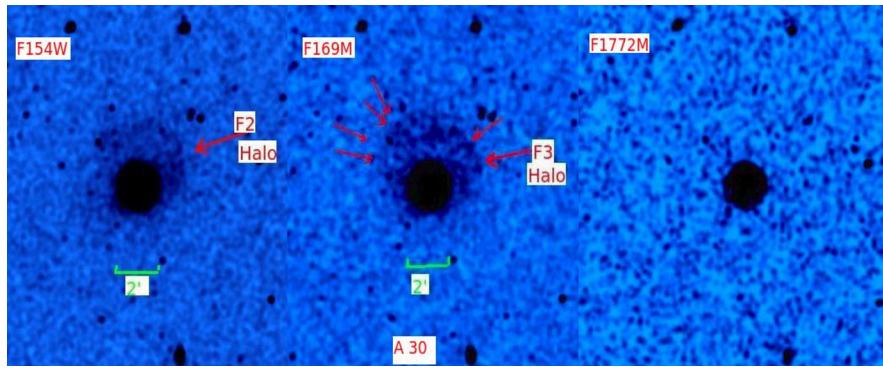


Figure 12. Images of A30 in F154W, F169M and F172M showing the FUV halo around F154 and F169M images and the absence of it around F172M image.

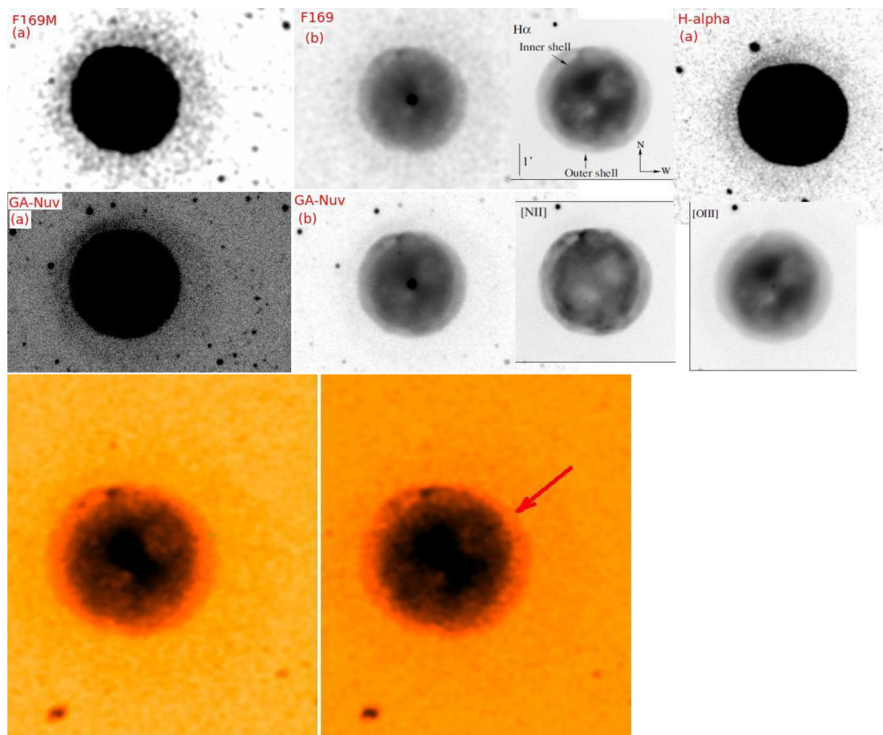


Figure 13. *Top:* Images of NGC 3587 (Owl Nebula) in F169M and GaleX NUV showing the halos around the deep images (marked as (a)). The nebula in F169M and GaleX NUV with two shells shown are marked as (b). Ground-based H α , [N II] and [O III] images (from Garcia-Diaz *et al.* 2018) are shown for comparison with UV images. The features of F169M and GaleX NUV are similar to [O III] and H α respectively. *Bottom:* Image of NGC 3587 in F154W (*left*) and F169M (*right*). F169M image shows a jet-like feature (shown by the arrow) that is absent in F154W image.

that is not seen either in F154W or F172M or even NUV images. This could be a hot [He II] emitting jet, a real sign of activity in a docile nebula.

2.2.5 EGB6. EGB 6 (PN G221.6+46.4) is a large ($13' \times 11'$) and very low-surface-brightness planetary nebula, serendipitously discovered by Bond on POSS prints in 1978. The central star, PG 0950+139 is a very hot DAOZ white dwarf with $T_{\text{eff}} = 105000 \pm 5000$ K, $\log_g = 7.4 \pm 0.4$ (Werner *et al.* 2018). The

CSPN has an apparent cool dwarf companion shrouded in dust at a separation of $0.''16$, which was initially detected through near infrared excesses (Bond *et al.* 2016). Initial spectroscopic observations showed the central star has strong [O III] emission. Later Liebert *et al.* (1989) showed that the strong [O III] nebular lines arise from a compact emission knot (CEK), which is unresolved and appears to coincide with the PNN in ground-based images. However, recent HST observations (Bond *et al.* 2016) showed

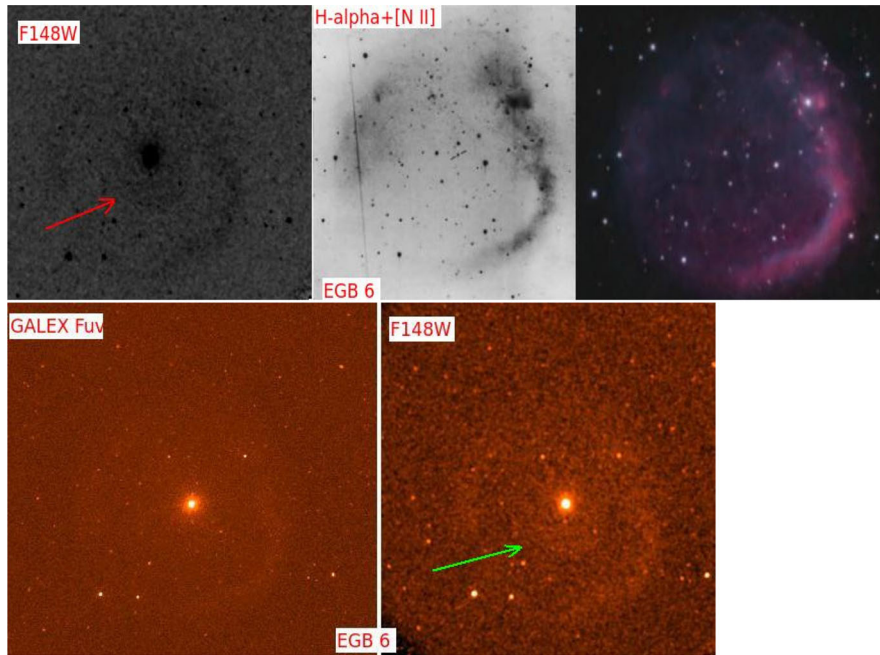


Figure 14. *Top:* UVIT image of EGB 6 in F148W filter showing the fainter outer nebula and smaller central nebula (shown by the arrow) along with an optical image of EGB 6 in H α and [N II] (Jacoby & Van De Steene 1995) and an optical colour image of the outer nebula from Don Goldman (astrodonimaging.com). Note that the inner smaller nebula is not present in the two optical images. *Bottom:* Galex FUV image of EGB 6 (*left*) is compared with UVIT image in F148W. The inner small nebula is shown by the arrow (*right*). Note the absence of inner small nebula in the GALEX image.

that even the emission knot is associated with a companion at $0.''166$ away from the CSPN. This corresponds to a projected linear separation of ~ 118 AU, for a nominal distance of about 725 pc. The electron density of the CEK is remarkably high, about $2.2 \times 10^6 \text{ cm}^{-3}$, according to an emission-line analysis by Dopita and Liebert (1989).

Thus, EGB 6 raises several astrophysical puzzles, including how to explain the existence and survival of a compact dense [O III] emission nebula apparently associated with a cool M dwarf, located at least 118 AU from the source of ionizing radiation (Bond *et al.* 2016). It is to be noted that very weak [O III] $\lambda 5007$ emission attributed to the large PN has been detected serendipitously in the SDSS spectra of two faint galaxies that happen to lie behind EGB 6 (Yuan & Liu 2013). Ackers *et al.* (1992) listed the relative intensities of H α , H β , and 5007 \AA .

Bond *et al.* (2016) suggested a scenario in which the EGB 6 nucleus is descended from a wide binary similar to the Mira system, in which a portion of the wind from an AGB star was captured into an accretion disk around a companion star; a remnant of this disk has survived to the present time and is surrounded by gas photoionized by UV radiation from the WD.

Our UVIT observation include imaging EGB 6 in F148W, F154W, F169M and F172M filters. The low surface brightness PN is present in all the filters with about same dimensions and appearance as the H α and [N II] images (Jacoby & Van De Steene 1995). The south-west part of the nebula is the brightest and even the F148 image shows wavy appearance which coincides with proper motion direction of the star.

The most interesting and unique structure that is only present in FUV filters F148W, F154W and F169M is a smaller nebula close to the CSPN extending to about $2.''4$ away from it. It has a bow-like appearance away from the central star (Figures 12 and 13) in the general direction of proper motion of the star. This central nebula is not even present in GALEX image. The existence of this small nebula adds a new puzzle to the already listed ones by Bond *et al.* (2016).

2.3 Elliptical nebulae

The members of this group from Table 1 are A 21, Jr Er 1, LoTr5, A70, Hu 1-2 and NGC 7293. Reduced Level 2 data of LoTr5, Jr Er1, A 70, Hu 1-2 is not

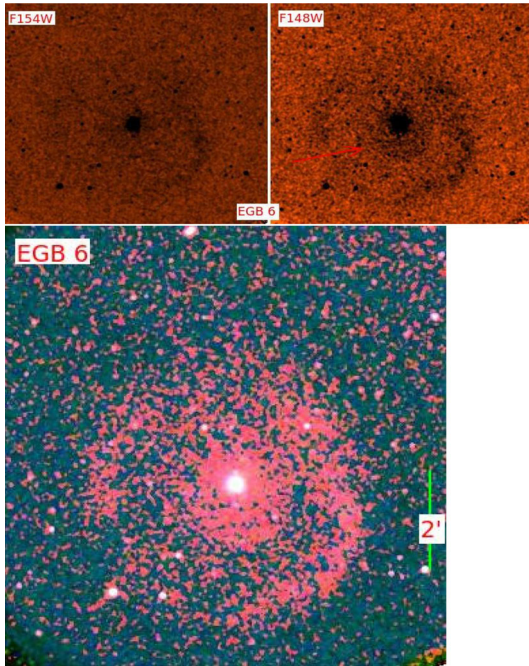


Figure 15. *Top:* UVIT image of EGB 6 in F154W filter showing the faint outer nebula and smaller central nebula along with F148W image of the outer nebula. Note that an inner smaller nebula is present in the two FUV images. *Bottom:* FUV image of EGB 6 in F148W. Note that the bow of the inner small nebula is towards South-West direction.

available. We present the results on three PNs A21, and NGC 7293 in the following sections.

2.3.1 *Abell 21, medusa nebula, A21.* A21 (PNG205.1+14.2) is a very wide ($685'' \times 530''$) evolved PN with a very hot white dwarf central star WD0726+133 also known as YM29. The T_{eff} and $\log g$ of the CSPN are estimated to be 140000 K and 6.5 respectively.

The WD central star appears as a point source superposed on diffuse emission in the MIPS 24 μm image (Chu *et al.* 2009). The flux density in the MIPS 24 μm band is almost three orders of magnitude higher than the expected photospheric emission. However, WD 0726+133 remains as a puzzle since no companion has been detected (Ciardullo *et al.* 1999). The IR excess is attributed to a dust disk. The origin of the dust is unclear whether it is accreted material or remnants of the dusty AGB phase. Whether the star is a binary is also a possibility (Clayton *et al.* 2014). A21 shares this property with JrEr 1 and NGC 7293.

Short exposure UVIT observations have been obtained in F169M and F172M in FUV and N263M and N245 in NUV filters. The central star as expected is conspicuous. The images are very similar to the

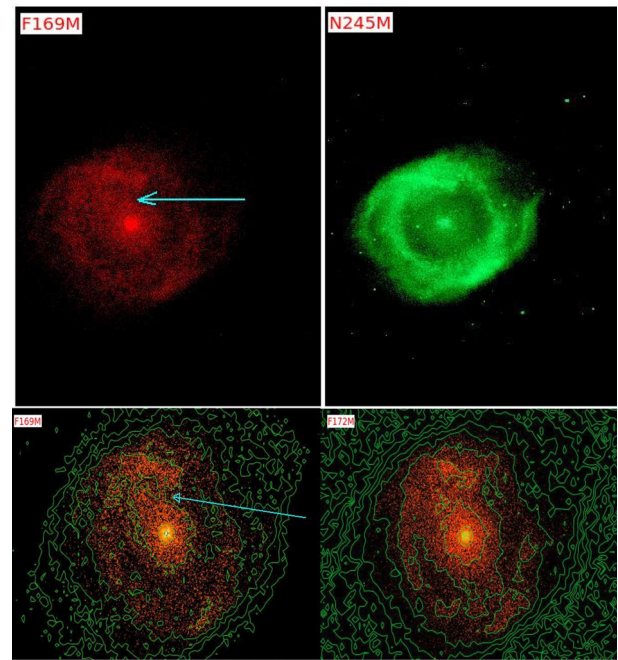


Figure 16. *Top:* UVIT image of NGC 7293 in F169M filter (red) showing the outer nebula and the [He II] filament (marked by arrow) connecting the central region (and the star). The *top right panel* shows the absence of [He II] filament in the N245M image. *Bottom:* Inner $4'$ regions of NGC 7293 in F169M (*left*) and F172M (*right*) superposed with intensity contours. The [He II] filament is seen in the F169M image (marked by arrow) whereas it is absent in the F172M image.

optical ones. The NUV images show great similarity to $H\alpha$ image with a large number of filaments (Fig. 14). However the FUV images look more diffuse similar to [O III] $\lambda 5007$ image (Manchado *et al.* 1996a). The F169M (includes [He II] 1640 \AA and [C IV] 1540 \AA) image shows a faint filament connecting the central star. However better observations are required.

2.3.2 *NGC 7293, helix nebula.* Helix nebula (PNG036.1-57.1) is one of the nearest (Gaia distance of 201 pc) and well-studied PN in almost all wavelengths (O'Dell *et al.* 2004, 2005, 2007; Meaburn *et al.* 2005, 2008; Hora *et al.* 2006; Montez *et al.* 2015; Van De Steene *et al.* 2015). It is also the largest PN in the sky with a diameter of about $13.5'$. A wide variety of phenomena has been studied in this PN ranging from exotic molecules, to X-rays, number of intriguing structures, from small cometary knots to large-scale arcs, to bipolar outflows, dusty disks, shock fronts etc. The inner helical structure is composed of thousands of cometary

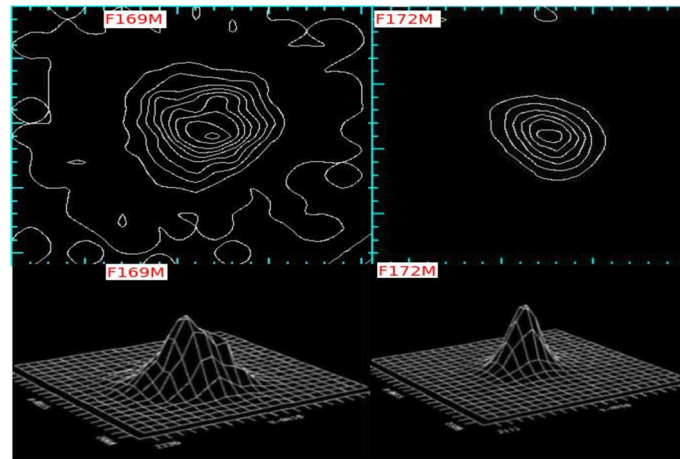


Figure 17. A surface and contour study of NGC 7293 in UVIT/FUV F169 and F172M bands. *Top:* Surface contours of the central source in F169 (*left*) and F172M (*right*) showing distorted contours for F169M indicating the possible presence of [He II] bright clouds or clumps around the CSPN. In F172M, the contours are more circular and suggests the presence of CSPN alone. *Bottom:* The figure shows the volume contours of the central source in F169M ([He II] emission line) and F172M (continuum) filters. The CSPN is seen to be accompanied by three [He II] clumps in F169M whereas the profile in F172M shows CSPN alone.

knots of lowly ionized and molecular gas (O’Dell *et al.* 2007; Etxaluze *et al.* 2014).

The white dwarf central star WD 2226-210 with a surface temperature of 103600 ± 5500 K (Napiwotzki 1999) ionizes the AGB nebula. Su *et al.* (2007) also showed the presence of a 35–150 AU diameter debris disk around this central star.

The main nebula consists of two rings of highly ionized gas and a faint outer filament. The three-dimensional (3D) structure of the main nebula has been investigated by Zeigler *et al.* (2013) who noted that the structure of the helix projects as if it were a thick walled barrel composed of red and blue-shifted halves in a bipolar geometry. The barrel axis of the helix is tilted about 10° East and 6° South relative to the line of sight.

There are two intriguing aspects that were revealed by infrared studies. Strong emission lines of [O IV] $25.9 \mu\text{m}$ and [Ne V] $24.3 \mu\text{m}$ have been detected in the Spitzer spectrum. This source of emission is identified with a point source centred on the CSPN. The excitation of [O IV] requires photons of 54.9 eV. In such a case, [He II] lines which also needs 54.4 eV for ionization (and recombination) are expected to produce a strong point source centered on the star. Images of [He II] $\lambda 4686$ have not shown such a point source. Secondly it has been known that Chandra X-ray imaging showed a hard X-ray point source, even at subarc second resolution, centered on the CSPN. The source of X-rays is unknown. The surface temperature of CSPN is not hot enough to generate hard X-rays

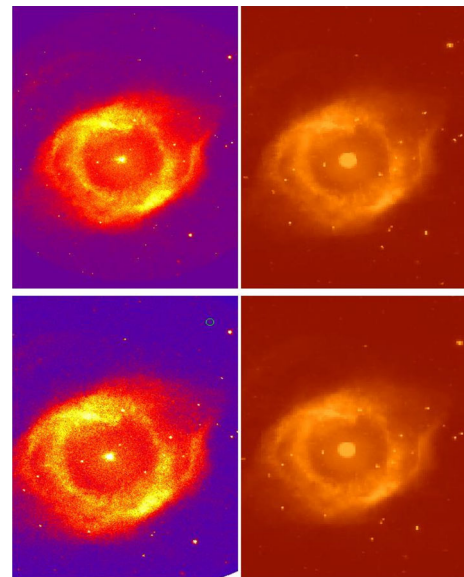


Figure 18. NUV image of NGC7293 in N245M (*left*) compared with GALEX NUV image. Image in N263M (*right*) is again compared with NUV GALEX image of NGC 7293. Note the higher spatial resolution of UVIT images and the radial filaments.

from its photosphere. FUV region contains [He II] 1640 \AA line, which is expected to be about 16 times stronger (recombination) than [He II] $\lambda 4686$, occurs in the F169M filter of UVIT. With a view to map the hot gas at higher spatial resolution ($1.''3$) we observed the central regions of helix nebula.

We observed the central region of helix in the first instance in two FUV filters F169M and F172M and

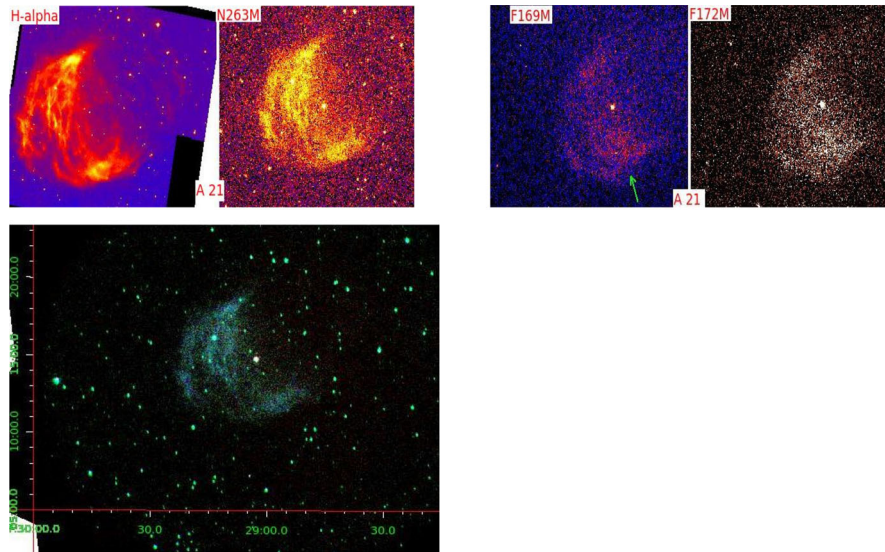


Figure 19. *Top left panel:* Images of A21 in H α (Manchado *et al.* 1996a) and in N263M showing the similarity of the filamentary structure. *Right panel:* The FUV images in F169M and F172M. The arrow points to the faint filament that connects to the CSPN. *Bottom:* UVIT composite image of A21 in three colours: F169M (blue), N263M (green) and N245M (red).

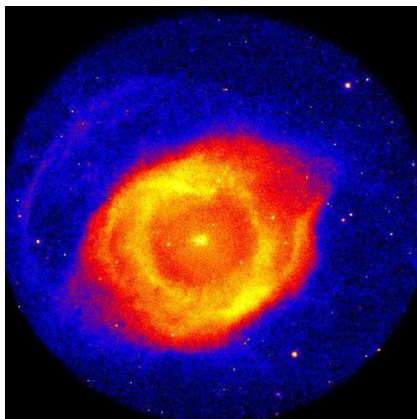


Figure 20. Details of UVIT image of NGC 7293 in the N263M filter. There are some new structures that are not seen in optical images.

two NUV filters N245M and N263M. F172M images expected to provide the continuum emission in contrast to F169M. NUV filters might include mostly the nebular continuum in addition to some low excitation emissions. IUE spectra up to 2 arc minutes away from CSPN show that [He II] 1640 Å line provides strongest emission in the inner regions. Figure 15 shows the relative comparison of the spatial resolution of UVIT with respect to GALEX both in FUV and NUV. Several nebular knots (cometary) seen in HST optical images (O’Dell *et al.* 2007) are also present in UV (Figures 16 and 17).

F169 images of the central region of helix showed mainly two surprising features in contrast to F172M (and N245M and N263M). The region around CSPN has nebulous clumps surrounding the point source

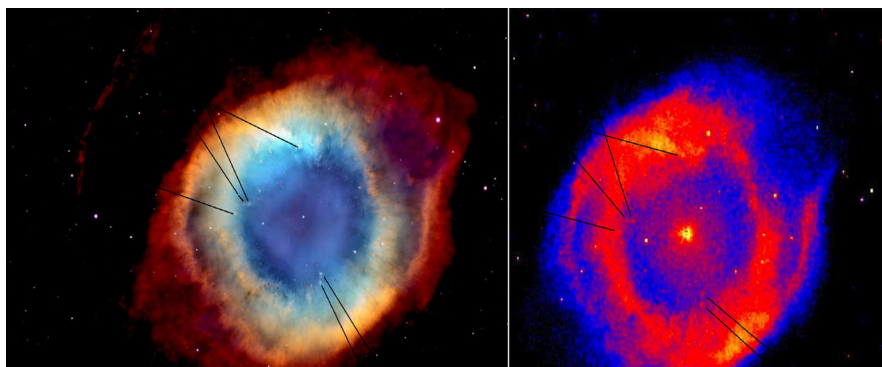


Figure 21. Details of UVIT image of NGC 7293 in the N263M filter. The fine optical knots detected in HST image (*left*) (O’Dell *et al.* 2005) are seen in the UV image in F263M (*right*) obtained with UVIT. The same knots are shown in both images. Some of the cometary knots are also present in UV images.

(Fig. 15). The intensity contours around the central source show few arc seconds extended regions suggesting that the central source is surrounded by clouds of [He II] (Fig. 18). Secondly, there is a nebulous streamer connecting the central region to the outer ring (Fig. 19). The [He II] streamers could possibly be providing mass flow to and from the central source. Could this be the source of accretion to the central WD?

Although NGC 7293 is of great astrophysical interest, it is not an easy object to observe because of its low surface brightness and its large angular extent in the sky. The field-of-view of UVIT is adequate to cover major portions of the nebula at any given pointing. We have observed two more locations in NGC 7293 covering the whole nebula including the shocked regions. Some of the data is not yet available. We hope to present a detailed paper later (Figures 20, 21).

3. Concluding remarks

In this paper, we have presented UVIT observations of 11 of the 19 proposed objects in our program. This compendium forms an “atlas” of sorts, of deep UV imaging of these objects, with a spatial resolution of $1''.5$. The data for the 8 objects is not yet available. The main theme that has been developed here is existence of the FUV halos. Halos around PN are well known and well studied (Ramos-Larios & Phillips 2009). For example, in NGC 3587, the halo is seen in all wavelengths from UV (Section 2.2.3) to the optical, and consists mainly of ionized gases (Guerrero & Manchado 1999). Extended ionized halo has been found around 60% of the PNs for which proper imaging has been done (Corradi *et al.* 2003). The halos are thought to be a result of mass-loss at the end of the AGB phase, their edges being the signature of the last thermal pulse (Steffen & Schnberner 2003). In contrast, the UVIT discovered FUV halos, and jets around bipolar nebulae and A 30 are only seen in wavelengths shortward of $\lambda 1650$ not in longer wavelength images. Warner and Lyman bands of H_2 start appearing shortward of $\lambda 1650$. Ultraviolet fluorescence spectra of H_2 as modeled by France *et al.* (2005) with IC 63, show strong emission peak at $\lambda 1608$ (λ_{eff} of F169M filter) and no emission shortward of $\lambda 1650$.

UVIT studies have brought out a totally new aspect to the hidden mass of the planetary nebulae namely existence of FUV halos, jets and arcs, mostly due to very cold H_2 gas around young, bipolar and even

some old PNs like born-again PNs as well. Such cold gas could only be seen through UV fluorescence of H_2 molecule. Big FUV lobes, and jets much bigger than optical nebulae have been detected through FUV studies by UVIT.

UV imaging in each case of PNs we studied, revealed a new aspect observationally which reiterates the importance of UV studies.

‘Planetary nebulae are like a box of chocolates, you never know what you are going to get’ – Monic Yourcg.

Acknowledgements

We would like to express our sincere thanks to several people who have helped us in carrying out this study of PNs, especially K. Sriram, Arturo Manchado for supplying ground based images of some the PN in nebular lines, Don Goldman for the colour image of EGB 6, and Annapurni Subramaniam for the contour images of NGC 7293. This publication uses the data from the AstroSat mission of the Indian Space Research Organisation (ISRO), archived at the Indian Space Science Data Centre (ISSDC). The publication uses UVIT data processed by the payload operations centre at IIA. The UVIT is built in collaboration between IIA, IUCAA, TIFR, ISRO and CSA. UVIT and AstroSat observatory development took about two decades before launch. Several people from several agencies were involved in this effort. We would like to thank them all collectively. NKR would like thank Department of Science and Technology for their support through grant SERB/F/2143/2016-17 ‘Aspects in Stellar and Galactic Evolution’. Some of the data presented in this paper (eg. GALEX, IUE, HST) were obtained from the Mikulski Archive for Space Telescopes (MAST). STScI is operated by the Association of Universities for Research in Astronomy Inc., under NASA contract NAS5-26555. Support for MAST for non-HST data is provided by the NASA Office of Space Science via grant NNX09AF08G and by other grants and contracts.

AKR acknowledges the support of the Raja Ramanna Fellowship of the Department of Atomic Energy prior to the submission of this work.

References

- Ackers A., Ochsenbein F., Stenholm B. *et al.* 1992, Strasbourg-ESO Catalogue of Galactic Planetary Nebulae

- Balick B. 1987, AJ, 94, 671
- Balick B., Frank A. 2002, ARAA, 40, 439
- Balick B., Frank A., Liu B., Huart-Espinosa H. 2017, ApJ, 843, 208
- Bianchi L. 2012, in Manchado A., Stanghellini L., Schonberner D., eds, Planetary Nebulae: An Eye to the Future, Proc. IAU Symp., 283, 45
- Bond H. E., Ciardullo R., Esplin T. L., Hawley S. A., Libert J., Munari U. 2016, ApJ, 826, 139
- Borkowski K. J., Harrington J. P., Tsvetanov Z. 1995, ApJ, 449, L143
- Borkowski K. J., Harrington J. P., Tsvetanov Z., Clegg R. E. S. 1993, ApJ, 415, 47
- Clayton G. C., De Marco O., Nordhaus J. *et al.* 2014, AJ, 147, 142
- Chu Y.-H., Chang T. H., Conway G. M. 1997, ApJ, 482, 891
- Chu Y.-H., Ho C.-H. 1995, ApJ, 448, 127
- Chu Y.-H., Grundl R. A., Conway G. M. 1987, AJ, 116, 1882
- Chu Y.-H., Kwitter K. B., Kaler J. B. 1993, AJ, 106, 650
- Chu Y.-H., Gruendi R. A., Conway G. M. 1998, AJ, 116, 1882
- Chu Y.-H., Su K. Y. L., Bilikov J. *et al.* 2011, AJ, 142, 75
- Chu Y.-H., Gruendl R. A., Guerrero M. A. *et al.* 2009, AJ, 138, 691
- Ciardullo R., Bond H. E., Sipior M. S., Fullton L. K., Zhang C.-Y., Schaefer K. G. 1999, AJ, 118, 488
- Corradi R. L. M., Schonberner D., Steffen M., Perinotto M. 2003, MNRAS, 340, 417
- Cox P., Huggins P. J., Maillard J.-P. *et al.* 2002, A&A, 384, 603
- Cuesta L., Phillips J. P. 2000a, ApJ, 543, 754
- Cuesta L., Phillips J. P. 2000b, AJ, 120, 2661
- Delfosse X., Kahane C., Forveille T. 1997, A&A, 320, 249
- De Marco O. 2009, PASP, 121, 316
- Dinerstein H. L., Lester D. F. 1984, ApJ, 281, 702
- Dopita M. A., Liebert J. 1989, ApJ, 347, 910
- Etxaluze M., Cernicharo J., Goicoechea J. R. *et al.* 2014, A&A, 566, 78
- Fang X., Guerrero M. A., Marquez-Lugo R. A., Toala J. A. *et al.* 2014, ApJ, 797, 100
- Feibelman W. A. 2001, ApJ, 550, 785
- France K., Andersson B.-G., McCandliss S. R., Feldman P. D. 2005, ApJ, 628, 750
- Garca-Segura G., Villaver E., Langer N., Yoon S.-C., Manchado A. 2014, ApJ, 783, 74
- Garcia-Diaz M. T., Steffen W., Henny W. J. *et al.* 2018, MNRAS, 479, 3909
- Gusten R., Wiesemeyer H., Neufeld D. 2019, Nature, 568, 357
- Guerrero M. A., Manchado A. 1999, ApJ, 522, 378
- Guerrero M. A., Ruiz N., Hamann W.-R. *et al.* 2012, ApJ, 755, 129
- Guerrero M. A., Chu Y.-H., Manchado A., Kwitter K. B. 2003, AJ, 125, 321
- Hazard C., Terlevich R., Morton D. C., Sargent W. L. W., Ferland G. 1980, Nature, 285, 463
- Hajian A. R., Frank A., Balick B., Terzian Y. 1997, ApJ, 477, 226
- Herald J. E., Bianchi L. 2011, MNRAS, 417, 2440
- Herwig F. 2005, ARA&A, 43, 435
- Hora J. L., Latter W. B., Smith H. A., Marengo M. 2006, 652, 426
- Hsia C.-H., Chau W., Zhang Y., Kwok S. 2014, 787, 25
- Hua C. T., Dopita M. A., Martinis J. 1998, A&AS, 133, 361
- Iben I. Jr., Kaler J. B., Truran J. W., Renzini A. 1983, ApJ, 264, 605
- Jacoby G. H. 1979, PASP, 91, 754
- Jacoby G. H., Van De Steene G. 1995, AJ, 110, 1285
- Jones D., Van Winckel H., Aller A., Exter K., De Marco O. 2017, A&A, 600, 9
- Kameswara Rao N., Sutaria F., Murthy J., Krishna S., Mohan R., Ray A. 2018, A&A, 609, L1
- Kameswara Rao N., De Marco O., Krishna S., Murthy J., Ray A., Sutaria F., Mohan R. 2018, A&A, 620, 138
- Kastner J. H., Vrtillek S. D., Soker N. 2001, ApJ, 550, 189
- Kastner J. H., Montez R. Jr., Balick B., *et al.* 2012, AJ, 144, 58
- Kemper F., Molster F. J., Jager C., Waters L. B. F. M. 2002, A&A, 394, 679
- Kumar A., Ghosh S. K., Hutchings J. *et al.* 2012, in Proc. SPIE., vol. 8443
- Kwitter K. B., Chu Y. H., Downes R. A. 1993, IAUS, 155, 209
- Kwok S., Purton C. R., Fitzgerald P. M. 1978, ApJ, 219, L125
- Lang D., Hogg D. W., Mierle K., Blanton M., Roweis S., 2010, AJ, 139, 1762
- Latter W. B., Kelly D. M., Hora J. L., Deutsch L. K. 1995, ApJS, 100, 159
- Lawlor T. M., MacDonald J. 2006, MNRAS, 371, 263
- Lester D. F., Dinerstein H. L. 1984, ApJ, 281, L67
- Liebert J., Green R., Bond H. E., Holberg J. B. *et al.* 1989, ApJ, 346, 251
- Lopez J. A., Vazquez R., Rodriguez L. F. 1995, ApJ, 455, L63
- Lopez J. A., Meaburn J., Bryce M., Holloway A. J. 1998, ApJ, 493, 803
- Lago P. J. A., Costa R. D. D. 2016, RmxAA, 52, 329
- Latter W. B., Dayal A., Bieging J. H., Meakin C. *et al.* 2000, ApJ, 539, 783
- Manchado A., Stanghellini L., Guerrero M. A. 1996a, ApJ, 466, L95
- Manchado A., Guerrero M. A., Stanghellini L., Serra-Ricart M. 1996b, The IAC Morphological Catalog of Northern Galactic Planetary Nebulae, IAC, La Laguna
- Mata H., Ramos-Larios G., Guerrero M. A. *et al.* 2016, MNRAS, 459, 841
- Matsuura M., Zijlstra A. A., Molster F. J., Waters L. B. F. M., Nomura H., Sahai R., Hoare M. G. 2005, MNRAS, 359, 383

- Martin C., Hurwitz M., Bowyer S. 1990, 354, 220
Masson C. R. 1989, *ApJ*, 336, 294
Meaburn J., López J. A. 1996, *ApJL*, 472, L45
Meaburn J., Lopez J. A., Steffen W., Graham M. F., Holloway A. J. 2005, *AJ*, 2005, 130, 2303
Meaburn J., Lopez J. A., Bryce M., Redman M. P. 1998, *A&A*, 334, 670
Meaburn J., Lloyd M., Vaytet N. M. H., Lopez J. A. 2008, *MNRAS*, 385, 269
Miller T. R., Henry R. B. C., Balick B. *et al.* 2019, *MNRAS*, 482, 278
Miller Bertolami M. M., Althaus L. G. 2006, *RMxAC*, 26, 48
Montez R. Jr., Kastner H., Balick B. *et al.* 2015, *ApJ*, 800, 8
Montez R., Kastner J. H. 2018, *ApJ*, 861, 45
Murthy J., Rahna P., Sutaria F. *et al.* 2017, *A&C*, 20, 120
Napiwotzki R., 1999, *A&A*, 350, 101
O'Dell C.R., McCullough P. R., Meixner M. 2004, *AJ*, 128, 2339
O'Dell C. R., Henney W. J., Ferland G. J. 2005, *AJ*, 130, 1720
O'Dell C. R., Henney W. J., Ferland G. J. 2007, *AJ*, 133, 2343
Peretto N., Fuller G. A., Zijlstra A. A., Patel N. A. 2007, *A&A*, 437, 207
Pittard J. M., Dyson J. E., Falle S. A. E. G., Hartquist T. W. 2005, *MNRAS*, 361, 1077
Rahana P. T., Murthy J., Safonova M. *et al.* 2017, *MNRAS*, 471, 3028
Ramos-Larios G., Phillips J. P. 2009, *MNRAS*, 400, 575
Ressler M. E., Cohen M., Wachter S. *et al.* 2010, *AJ*, 140, 1882
Santander-García M., Bujarrabal V., Alcolea J., Castro-Carrizo A., Sánchez Contreras C., Quintana-Lacaci G., Corradi R. L. M., Neri R. 2017, *A&A*, 597, 27
Schmidt D. R., Ziury L. M. 2016, *ApJ*, 817, 175
Seaton M. J. 1980, *QJRAS*, 21, 229
Singh K. P., Tandon S. N., Agrawal P. C. *et al.* 2014, *Proc. SPIE*, 9144, 91441S
Steffen M., Schnberner D. 2003, *IAUS*, 209, 439
Su K. Y. L., Chu Y.-H., Rieke G. H., Huggins P. J. *et al.* 2007, *ApJ*, 657L, 41
Szyszka C., Walsh J. R., Zijlstra A. A., Tsamis Y. G. 2009, *ApJ*, 707, L32
Szyszka C., Zijlstra A. A., Walsh J. R. 2011, *MNRAS*, 416, 715
Tandon S. N., Hutchings J. B., Gosh S. K. *et al.* 2017a, *JApA*, 38, 28
Tandon S. N., Subramaniam A., Girish V. *et al.* 2017b, *AJ*, 154, 128
Tandon S. N. *et al.* 2020, *AJ*, 159, 158
Tarafdar S. P., Apparao K. M. V. 1988, *ApJ*, 327, 342
Toalá J. A., Guerrero M. A., Todt H. *et al.* 2015, *ApJ*, 799, 67
Van De Steene G. C., Van Hoof P. A. M., Exter K. M., Barlow M. *et al.* 2015, *A&A*, 574, 134
Vazquez R. 2012, *ApJ*, 751, 116
Walton N. A., Pottasch S. R., Reay N. K. 1988, *A&A*, 200, 21
Wang M.-Y., Muthumariappan C., Kwok S. 2006, *IAUS*, 234, 537
Wang M.-Y., Hasegawa T. I., Kwok S. 2008, *ApJ*, 673, 264
Werner K., Rauch T., Kruk J. W. 2018, *A&A*, 616, 73
Werner K., Rauch T., Reindl N. 2019, *MNRAS*, 483, 5291
Wesson R., Cernicharo J., Barlow M. J. *et al.* 2010, *A&A*, 518, 144
Witt A. N., Stecher T. P., Boroson T. A., Bohlin R. C. 1989, *ApJ*, 336, L21
Wright N. J., Barlow M. J., Ercolano B., Rauch T. 2011, *MNRAS*, 418, 370
Yuan H. B., Liu X. W. 2013, *MNRAS*, 436, 718
Zeigler N. R., Zack L. N., Woolf N. J., Ziurys L. M. 2013, *ApJ*, 778, 16
Zhang Y., Liu X.-W., Luo S. G., Péquignot D., Barlow M. J. 2005, *A&A*, 442, 249
Zijlstra A. A., Van Hoof P. A. M., Perley R. A. 2008, *ApJ*, 681, 1296